Int. J. Heat Mass Transfer. Vol. 28, No. 8, pp. 1451–1460, 1985
Printed in Great Britain

0017-9310/85 $3.00 + 0.00

Analysis of evaporation in the presence of composition-induced natural convection

E. M. SPARROW, G. A. NUNEZ and A. T. PRATA
Department of Mechanical Engineering, University of Minnesota, Minneapolis, MN 55455, U.S.A.

(*Received* 6 *December* 1984 *and in final form* 12 *February* 1985)

Abstract—Evaporation from an open-topped vertical tube which is partially filled with a liquid has been investigated analytically and numerically. The space above the liquid surface is occupied by a binary mixture consisting of the evaporating vapor and a gas. Spatial variations of the concentrations of the vapor and the gas give rise to density variations which induce natural convection motions. The numerical solutions were carried out for water as the evaporating vapor and air as the gas. It was found that the presence of natural convection can lead to significant increases in the rate of evaporation—up to a factor of five for the investigated parameter ranges. The enhancement is favored by a relatively high concentration of vapor at the liquid surface, a dry ambient, and a relatively large tube diameter. The flow pattern consists of a U-shaped loop, with fluid drawn downward into the tube from the ambient through an annular region adjacent to the tube wall. The upstreaming flow in the core of the tube forms the other leg of the loop.

INTRODUCTION

THIS PAPER is concerned with the natural convection that is induced in a binary gas–vapor mixture due to evaporation at a liquid surface which bounds the mixture from below. The physical situation to be considered is an open-topped circular tube that is partially filled with a volatile liquid. In the ambient at the top of the tube, the composition, pressure, and temperature of the binary mixture are time invariant. The partial pressure of the vapor in the ambient is maintained at a lower value than that at the liquid surface, so that evaporation occurs.

The temperature condition was chosen to be the same as that of the classical Stefan diffusion problem [1–4]. This choice was made to enable the results of the Stefan problem to be used as a baseline for comparison with the present results. Since natural convection is neglected in the Stefan problem but is included here, deviations between the two sets of results may be attributed to the action of natural convection.

The Stefan diffusion problem is isothermal. Procedures for the attainment of isothermal conditions are well documented in the literature because the results of the Stefan problem are widely used as the basis for an experimental method for determining the mass diffusion coefficient [5, 6].

Consistent with the isothermal model, density variations in the binary gas–vapor mixture are necessarily due to variations in the concentrations of the components which make up the mixture. Owing to evaporation at the surface of the liquid, such concentration variations will exist. If the molecular weight of the evaporating vapor is greater than that of the gas, the mixture density will decrease in the upward vertical direction. On the other hand, if the evaporating vapor has a lower molecular weight than the gas, there will be a vertical upward increase of density. The latter situation is unstable and gives rise to natural convection motions in the binary gas mixture. It is, therefore, the situation which will be investigated here. In particular, the numerical work will be performed for water as the evaporating vapor and air as the gas.

Several parameters were varied during the course of the research. One of these is the Grashof number suitably defined for natural convection mass transfer. Another is the length–radius ratio of the portion of the tube between the surface of the liquid and the open top. Although not strictly a parameter, the closure condition at the top of the tube was explored in a parameter-like manner in order to establish its effect on the results.

Among the results, the quantity of main interest is the rate of evaporation. The natural-convection-affected evaporation rates will be compared with those from the Stefan diffusion problem. To further document the role of natural convection, velocity profiles, mass fraction profiles, and streamline maps will be presented.

A literature survey failed to reveal any prior studies of natural convection in mass transfer problems of the Stefan type. In the one investigation where density variations were considered, the molecular weight of the evaporating vapor was greater than that of the gas, so that natural convection did not occur [7].

ANALYSIS

The description of the analysis is facilitated by reference to the inset of Fig. 1, which is a diagram showing the coordinates and dimensional nomenclature. The problem will be formulated in (x, r) cylindrical coordinates, with axisymmetry assumed to prevail. In common with the Stefan model, the analysis will be

NOMENCLATURE

D	tube diameter
$\mathscr{D}$	mass diffusion coefficient
f_B	buoyancy per unit mass
Gr	Grashof number, equation (12)
g	acceleration of gravity
L	distance between liquid surface and tube opening
M	molecular weight
$\dot{m}$	evaporation rate
P	dimensionless pressure, equation (6)
p	pressure
p'	rescaled pressure, $(p+\rho_\infty gx)$
R	tube radius
$\bar{R}$	universal gas constant
Re	evaporation Reynolds number, $4\dot{m}/\mu\pi D$
r	radial coordinate
Sc	Schmidt number
T	temperature
U, V	dimensionless velocities, equation (6)
u, v	velocity components
W	mass fraction
X	dimensionless axial coordinate, x/L
x	axial coordinate.

Greek symbols

η	dimensionless radial coordinate, r/R
θ	dimensionless mass fraction, $(W_1-W_{1\infty})/(W_{10}-W_{1\infty})$
μ	viscosity
ν	kinematic viscosity
ρ	density.

Subscripts

0	at the liquid surface
1	component 1, vapor
2	component 2, gas
∞	in the ambient.

carried out on a quasi-steady basis, so that time-dependent terms do not appear in the conservation equations or the boundary conditions.

Governing equations

The key feature of the analysis is the buoyancy term which appears in the x-momentum equation. At any point (x, r), the local buoyancy force f_B per unit mass can be written as

$$\rho f_B = -\partial p/\partial x - \rho g. \tag{1}$$

If the quantity $\rho_\infty g$ is added and subtracted on the RHS of equation (1) and if $p' = (p+\rho_\infty gx)$, then

$$\rho f_B = -\partial p'/\partial x - \rho g(1-\rho_\infty/\rho) \tag{2}$$

in which ρ and ρ_∞ respectively denote the densities of the mixture at (x, r) and in the ambient at the open top of the tube.

The mixture will be treated as a perfect gas, so that

$$\rho = p/(\bar{R}/M)T, \quad \rho_\infty = p_\infty/(\bar{R}/M_\infty)T_\infty. \tag{3}$$

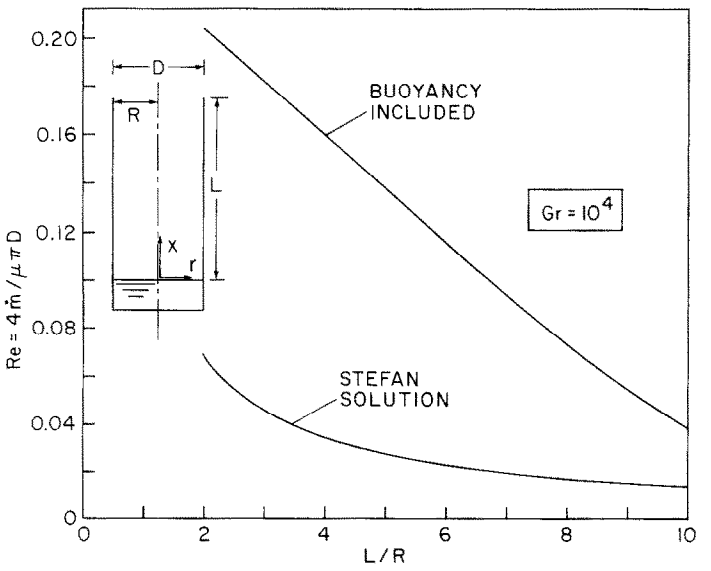

FIG. 1. Evaporation rates for $W_{10} = 0.04$, $W_{1\infty} = 0$ and $Gr = 10^4$. The inset illustrates the physical situation.

Since the variation of the pressure is very much smaller than the variation of the molecular weight and since the temperature is uniform, it follows that $\rho_\infty/\rho = M_\infty/M$. The mixture molecular weight can be expressed in terms of the molecular weights M_1 and M_2 of the components 1 and 2 (the vapor and the gas, respectively) and of their mass fractions W_1 and W_2

$$M = M_1 M_2/(W_1 M_2 + W_2 M_1). \tag{4}$$

With this and noting that $W_1 + W_2 = 1$, it follows that

$$1 - \rho_\infty/\rho = (W_{1\infty} - W_1)/[W_{1\infty} + M_1/(M_2 - M_1)]. \tag{5}$$

The substitution of equation (5) into equation (2) yields the final expression for the buoyancy force.

Attention will now be turned to the equations which express mass, momentum, and species conservation. In writing these equations, the fluid properties will be treated in a manner identical to that employed for thermal natural convection, namely, the density variations are accounted only in the formulation of the buoyancy force and, thereafter, all fluid properties are taken to be constant. In addition, dimensionless variables are introduced in accordance with the definitions

$$U = uR/\nu, \quad V = vR/\nu, \quad P = p'/\rho(\nu/R)^2, \quad \theta = (W_1 - W_{1\infty})/(W_{10} - W_{1\infty}) \tag{6}$$

$$X = x/R, \quad \eta = r/R \tag{7}$$

where W_{10} and $W_{1\infty}$ are the mass fractions of the vapor at the surface of the liquid and in the ambient.

With these and with the foregoing expression for the buoyancy force, the conservation equations can be written as:

continuity (mass conservation for mixture)

$$\partial U/\partial X + \partial V/\partial \eta + V/\eta = 0, \tag{8}$$

x-momentum

$$U(\partial U/\partial X) + V(\partial U/\partial \eta) = -\partial P/\partial X + Gr\theta + \nabla^2 U, \tag{9}$$

r-momentum

$$U(\partial V/\partial X) + V(\partial V/\partial \eta) = -\partial P/\partial \eta + \nabla^2 V - V/\eta^2, \tag{10}$$

conservation of component 1

$$U(\partial \theta/\partial X) + V(\partial \theta/\partial \eta) = (1/Sc)\nabla^2 \theta. \tag{11}$$

Equations (8)–(11) constitute a coupled nonlinear system for the four variables U, V, P, and θ. The two prescribable parameters appearing in these equations are the Schmidt number Sc and the Grashof number Gr. The definition of the latter arises naturally from the variables of the analysis as

$$Gr = g\beta'(W_{10} - W_{1\infty})R^3/\nu^2 \tag{12}$$

$$\beta' = [W_{1\infty} + M_1/(M_2 - M_1)]^{-1} \cong (M_2 - M_1)/M_1 \tag{13}$$

where the right-hand member of equation (13) is included to call attention to the fact that $W_{1\infty}$ is usually very small compared with $M_1/(M_2 - M_1)$.

Boundary conditions

The boundary conditions at the surface of the liquid ($x = 0$) will be considered first. The surface will be regarded as being impermeable to the gas (component 2). In accordance with the impermeability condition, the naturally occurring diffusive flow of gas to the interface (diffusion from higher to lower concentration) must be balanced by a convective flow of gas away from the interface. This balance between convection and diffusion yields (at $x = 0$ and any r)

$$\rho_2 u = \rho \mathscr{D}(\partial W_2/\partial x) \tag{14}$$

where $\mathscr{D}$ is the mass diffusion coefficient. Since $W_2 = 1 - W_1$ and $\partial W_2/\partial x = -\partial W_1/\partial x$, equation (14) becomes

$$U = -[(W_{10} - W_{1\infty})/(1 - W_{10})Sc](\partial \theta/\partial X) \quad \text{at} \quad X = 0 \tag{15}$$

in which the dimensionless variables of equation (6) have been employed. Equation (15), which relates the velocity normal to the liquid surface to the gradient of the vapor mass fraction, will serve as the boundary condition for the velocity.

In considering the radial velocity $v(0, r)$ at the interface, it may first be noted that the diffusive fluxes in the radial direction are zero since $\partial W_1/\partial r = -\partial W_2/\partial r = 0$ (W_1 and W_2 are uniform at the interface). Because of this, no physical principles are violated by employing the no-slip condition, so that

$$V = 0 \quad \text{at} \quad X = 0. \tag{16}$$

Finally, the specification that $W_1 = \text{constant} = W_{10}$ at the interface yields

$$\theta = 1 \quad \text{at} \quad X = 0. \tag{17}$$

Attention is now turned to the boundary conditions at the tube wall, $r = R$ and $\eta = 1$. The wall is impermeable to both the gas and vapor, giving rise to balances between the convective and diffusive fluxes

$$\rho_1 v = \rho \mathscr{D}(\partial W_1/\partial r), \quad \rho_2 v = \rho \mathscr{D}(\partial W_2/\partial r) \tag{18}$$

so that

$$(\rho_1 + \rho_2)v = \rho \mathscr{D}(\partial W_1/\partial r + \partial W_2/\partial r) = 0 \tag{19}$$

from which it follows that $v = 0$ or that

$$V = 0 \quad \text{at} \quad \eta = 1. \tag{20}$$

Also, with $v = 0$, equation (18) shows that $\partial W_1/\partial r = 0$ and $\partial W_2/\partial r = 0$, which yields

$$\partial \theta/\partial \eta = 0 \quad \text{at} \quad \eta = 1. \tag{21}$$

The validity of the no-slip condition for the axial velocity component $u(R, x)$ at the wall is still uncertain (e.g. [8]) because of the non-zero diffusive fluxes in the axial direction (i.e. $\partial W_1/\partial x = -\partial W_2/\partial x \neq 0$). On the other hand, there does not appear to be an accepted mathematical description of the slip velocity, if such a velocity exists. In the present problem, the use of the no-slip boundary condition is conservative in that it tends

to diminish the effect of the natural convection. On this basis, the no-slip condition will be imposed, so that

$$U = 0 \quad \text{at} \quad \eta = 1. \tag{22}$$

The last set of boundary conditions to be specified are those at the top of the tube, $x = L$ and $X = L/R$. For the velocity problem,

$$\partial U/\partial X = 0, \quad V = 0 \quad \text{at} \quad X = L/R. \tag{23}$$

These closure conditions do not impose significant constraints on the velocity field as a whole provided that the finite-difference grid used in the numerical solution of the problem is closely packed near the top of the tube.

In formulating the boundary condition for the mass fraction, it is relevant to note that the natural convection may induce an inflow from the ambient into the tube through a portion of the cross section at $x = L$. The inflow will carry the vapor mass fraction $W_{1\infty}$. On the other hand, the fluid which exits the tube through $x = L$ may carry a different vapor mass fraction. To accommodate this situation, the so-called inflow/outflow boundary condition was formulated, whereby $W_1 = W_{1\infty}$ if $u < 0$ and $\partial W_1/\partial x = 0$ if $u > 0$. In dimensionless terms,

$$\theta = 0 \quad \text{if} \quad U < 0, \quad \partial\theta/\partial X = 0 \quad \text{if} \quad U > 0 \quad \text{at} \quad X = L/R \tag{24}$$

The sensitivity of the results to the W_1 closure condition was explored by employing the alternative condition that $W_1 = W_{1\infty}$ over the entire cross section at $x = L$, or that

$$\theta = 0 \quad \text{at} \quad X = L/R \tag{25}$$

which completes the formulation of the boundary conditions.

Numerical solutions

The governing differential equations (8)–(11) and their boundary conditions were solved as an adaptation of an elliptic finite-difference scheme (SIMPLER) set forth in [9], with the block correction of [10] incorporated to speed convergence of the iterative procedure. The computations were performed on a 30×21 non-uniform grid, respectively in the axial and radial directions. For the layout of the grid, a two-step process was employed. First, solutions were obtained with a uniform grid. Then, based on the velocity distributions from these solutions, the grid was redeployed on a point-by-point basis in order to accommodate locally rapid variations (e.g. boundary layers).

As is standard for elliptic-type natural convection problems, substantial under-relaxation was required to achieve convergence. Convergence was also aided by first running solutions for a sparse grid and then using these solutions as input to a refined grid, whose solutions were, in turn, used as input to a still finer grid.

The parameterization of the solutions will now be discussed. As noted in the Introduction, the numerical solutions were performed for water as the evaporating vapor and air as the gas. For this system, the Schmidt number Sc is 0.6.

Two distinctive cases were considered with respect to the mass fractions W_{10} and $W_{1\infty}$. The first case was characterized by $W_{10} = 0.04$ and $W_{1\infty} = 0$, with an associated $Gr = 10^4$ (tube diameter $D \sim 1.5$ in). This value of W_{10} corresponds to saturated vapor at a temperature just under 100°F and to a system pressure of 1 atm, while $W_{1\infty} = 0$ denotes a completely dry ambient. For the second case, $W_{10} = 0.04$ and $W_{1\infty} = 0.036$, with an associated value of $Gr = 10^3$. This $W_{1\infty}$ value corresponds to an ambient relative humidity of 90%. Thus, the distinction between the two cases is that the ambient is bone dry in one and very humid in the other, with an order of magnitude difference in the Grashof numbers reflecting the change in $(W_{10} - W_{1\infty})$.

For each of these cases, numerical solutions were carried out for seven values of the tube aspect ratio L/R between 2 and 10. Furthermore, at each aspect ratio, separate solutions were obtained for the two mass fraction closure conditions described by equations (24) and (25).

RESULTS AND DISCUSSION

The presentation of results will begin with the rate of evaporation—the quantity that is most relevant to practice. Subsequently, to provide further insights, velocity profiles, streamline maps, and mass fraction profiles will be presented.

Rate of evaporation

The rate of evaporation at a differential area dA on the liquid surface ($x = 0$) can be written as

$$[\rho_1 u - \rho\mathscr{D}(\partial W_1/\partial x)]\, dA \tag{26}$$

where both the convective and diffusive contributions have been included. By making use of equation (14) with $\partial W_2/\partial x = -\partial W_1/\partial x$ and noting that $\rho = \rho_1 + \rho_2$, the expression in equation (26) becomes

$$\rho u\, dA \tag{27}$$

and $dA = 2\pi r\, dr$. With these, the rate of evaporation $\dot{m}$ from the entire surface of the liquid can be written as

$$\dot{m} = \int_0^R \rho u 2\pi r\, dr. \tag{28}$$

A meaningful dimensionless representation can be obtained by incorporating $\dot{m}$ into the Reynolds number which, for a tube flow, is

$$Re = 4\dot{m}/\mu\pi D. \tag{29}$$

Upon combining equations (28) and (29) and using the variables of the analysis, there follows

$$Re = 4\int_0^1 U\eta\, d\eta. \tag{30}$$

Equation (30) was evaluated using the numerical solutions.

The evaporation rate results obtained from the present analysis will be compared with those of the Stefan diffusion problem, where natural convection is not taken into account. For reference purposes, the dimensionless evaporation rate for the Stefan solution is presented here

$$Re = [2(M_1/M)/Sc(L/R)] \ln(1+\Omega) \quad (31)$$

$$\Omega = [(W_{10}-W_{1\infty})/(1-W_{10})] \div [(1-W_{1\infty})(M_1/M_2)+W_{1\infty}]. \quad (31a)$$

A difficulty is encountered in the numerical evaluation of equation (31) in that the mixture molecular weight M varies along the tube. The Stefan model provides no guidelines about how to evaluate M. Here, mean values of W_1 and W_2 are defined as

$$\bar{W}_1 = \tfrac{1}{2}(W_{10}+W_{1\infty}), \quad \bar{W}_2 = 1-\bar{W}_1 \quad (32)$$

and M is evaluated from equation (4) with these mean values as input.

The numerical results for the evaporation rate are presented in Figs. 1 and 2, respectively for $Gr = 10^4$ and 10^3. In each figure, the evaporation Reynolds number is plotted as a function of the tube aspect ratio L/R. Curves are included which represent the present results (buoyancy included) and those of the Stefan solution. The issue of the mass fraction closure condition has been left open in the figures but will be discussed shortly.

Examination of the $Gr = 10^4$ results of Fig. 1 shows that the evaporation rates in the presence of natural convection are very much greater than those for the Stefan problem, which are due to diffusion alone. The enhancement stems from the dominance of the buoyancy-driven convective motions, yielding evaporation rates that are 3–5 times the Stefan values. Such large enhancements are reflective of a class of operating conditions characterized by a relatively high concentration of the water vapor at the liquid surface, a very dry ambient, and a relatively large tube radius (reflected in the magnitude of the Grashof number). Clearly, it is inappropriate to use the Stefan model to predict evaporation rates for such conditions.

The evaporation results for $Gr = 10^3$ in Fig. 2 convey a different message. Here, the with-buoyancy evaporation rates are, for all practical purposes, the same as those for the Stefan problem. The fact that the natural convection is ineffectual in this case is due to the small difference between the vapor mass fractions at the liquid surface and in the ambient (i.e. $W_{10}-W_{1\infty} = 0.004$), as also reflected by the value of Gr ($=10^3$). Thus, the validity of the Stefan solution can be ensured by operating with small values of $W_{10}-W_{1\infty}$.

The influence of the alternative mass fraction closure conditions [equations (24) and (25)] on the evaporation results will now be discussed. For the operating conditions of Fig. 1, the evaporation rates corresponding to the respective closures are virtually the same within the resolution of the figure. As will be elaborated later, the substantial inflow of dry air into the tube from the ambient, as occurs for these operating conditions, tends to bring the two boundary conditions together.

In Fig. 2, a slight difference in the evaporation rates associated with the alternative mass fraction closure conditions is in evidence. The uniform mass fraction closure, equation (25), yields results which coincide with the Stefan solution within the resolution of the figure, while the results for the inflow/outflow closure, equation (24), are slightly lower at certain L/R. That the alternative closure conditions are now more distinct than in the preceding case is due to the diminished inflow from the ambient into the tube for the operating conditions of Fig. 2. Note also that the uniform mass fraction closure is implicit in the Stefan model.

As a final observation in Figs. 1 and 2, it is seen that the evaporation rate decreases as the distance between

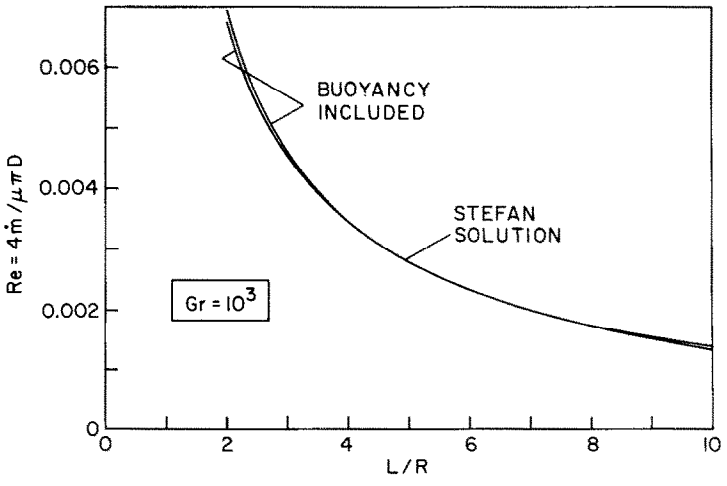

FIG. 2. Evaporation rates for $W_{10} = 0.04$, $W_{1\infty} = 0.036$ and $Gr = 10^3$.

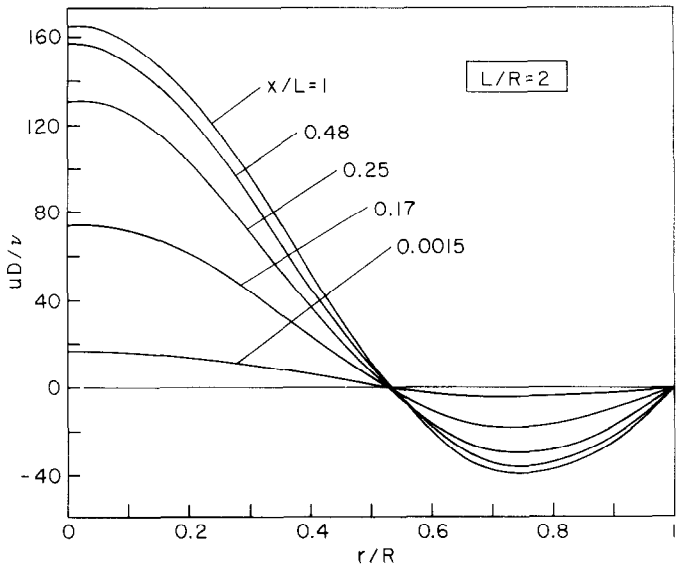

FIG. 3. Velocity profiles for a tube with aspect ratio $L/R = 2$. $W_{10} = 0.04$, $W_{1\infty} = 0$ and $Gr = 10^4$.

the liquid surface and the tube opening increases. This behavior reflects the increased resistance to mass transfer associated with the greater transport length. When natural convection plays a dominant role (Fig. 1), the evaporation rate decreases more rapidly with L/R than that for the Stefan solution. Consequently, the gap between the two curves diminishes at larger L/R.

Velocity field results

The velocity field information now to be presented includes both velocity profiles and streamline maps. The results for the buoyancy-dominated case ($W_{10} = 0.04$, $W_{1\infty} = 0$, $Gr = 10^4$) are particularly novel and will, therefore, be the focus of the presentation.

The evolution of the velocity field along the tube is respectively set forth in Figs. 3 and 4 for the shortest and longest of the investigated tube lengths, namely, $L/R = 2$ and 10. Each figure displays a succession of velocity profiles parameterized by the dimensionless axial coordinate x/L. On the ordinate, the velocity is embedded in the dimensionless group uD/ν, which can be regarded as a local Reynolds number. The profiles plotted in these figures correspond to the inflow/outflow mass fraction boundary condition [equation (24)], but they also apply with only slight deviations for the uniform mass fraction boundary condition [equation (25)].

The most noteworthy feature of Figs. 3 and 4 is the two-lobed nature of the velocity profiles. In the central core of the tube, which extends from the centerline ($r = 0$) to $r/R \sim 0.55$, the u velocity is positive, indicating a flow directed upward toward the open end of the tube. On the other hand, in the annulus which spans between the outer rim of the core and the tube wall, the flow is directed downward toward the bottom of the tube as witnessed by the negative values of u. This downward-directed flow is drawn into the open top of the tube from the ambient. It is interesting to note that the crossover from positive u to negative u occurs at virtually the same radial position at all axial stations and, in addition, the crossover point is hardly affected by the tube aspect ratio L/R.

Another significant feature of Figs. 3 and 4 is the magnitude of the velocities that are induced by the

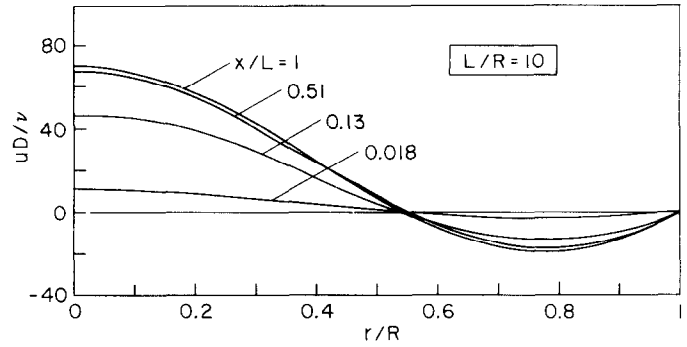

FIG. 4. Velocity profiles for a tube with aspect ratio $L/R = 10$. $W_{10} = 0.04$, $W_{1\infty} = 0$ and $Gr = 10^4$.

natural convection. To provide perspective for the velocity magnitudes displayed in these figures, it may be noted that the evaporation Reynolds numbers corresponding to $L/R = 2$ and 10 are approximately 0.2 and 0.04, respectively. The evaporation Reynolds number can be written as $\bar{u}D/v$, where $\bar{u}$ is the mean velocity of the *net* upflow. In Fig. 3, the maximum velocity occurs at the center of the open top of the tube and is characterized by $uD/v \cong 160$, which is very large compared with $\bar{u}D/v \cong 0.2$. The maximum velocity $uD/v \cong 70$ in Fig. 4 is also very large compared with $\bar{u}D/v \cong 0.04$.

From the foregoing, it is clear that a minimal portion of the flow which streams upward through the core is evaporated vapor. Rather, the overwhelming majority of the core flow consists of fluid that was drawn into the tube through the annulus. This indicates the presence of a U-shaped flow loop, with the downflow leg in the annulus and the upflow leg in the core.

Further inspection of Figs. 3 and 4 indicates an evolution of the velocity profiles which is virtually completed in the lower half of the tube. This observation can be verified by noting that there is very little change between the profiles for $x/L \cong 0.5$ and 1. The near congruence of the profiles in the upper half of the tube lends support to the imposed outflow conditions for the velocity [equation (23)].

A final observation in Figs. 3 and 4 relates to the response of the velocity magnitude to increases in tube length (i.e. to increasing L/R). Clearly, the greater hydrodynamic resistance associated with the longer tube of Fig. 4 causes a significant decrease in the velocities.

The patterns of fluid flow that were inferred during the preceding discussion are graphically displayed in Figs. 5 and 6 which are, respectively, the counterparts of Figs. 3 and 4. Each of Figs. 5 and 6 includes a pair of streamlined maps, respectively designated as (a) and (b).

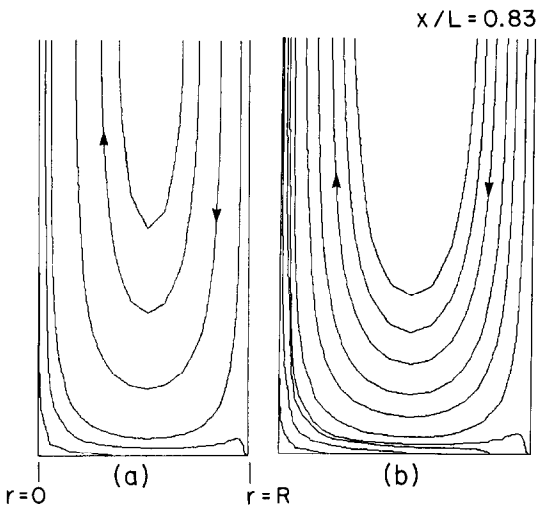

FIG. 5. Streamline maps for a tube with aspect ratio $L/R = 2$. $W_{10} = 0.04$, $W_{1\infty} = 0$ and $Gr = 10^4$.

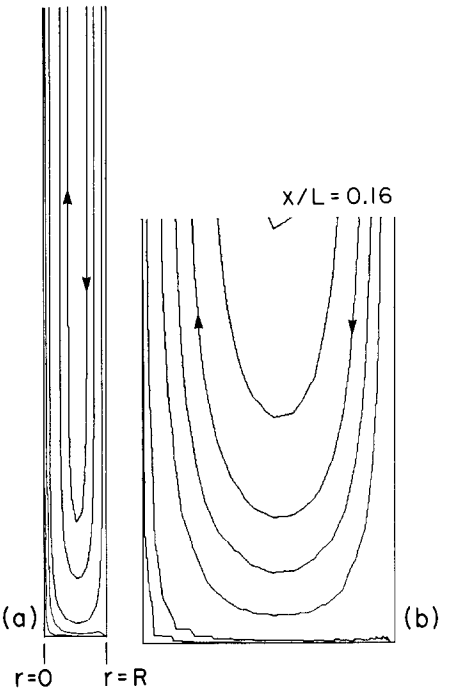

FIG. 6. Streamline maps for a tube with aspect ratio $L/R = 10$. $W_{10} = 0.04$, $W_{1\infty} = 0$ and $Gr = 10^4$.

The (a) part shows the streamlines in the tube as a whole, covering the region from $r = 0$ to $r = R$ and from $x = 0$ to $x = L$. The axial and radial lengths are to scale, respectively, 2 : 1 and 10 : 1 in Figs. 5(a) and 6(a). In the (b) part, the scales have been expanded in order to provide greater resolution of the flow field in the lower portion of the tube. In Fig. 5(b), the diagram terminates at $x/L = 0.83$, while Fig. 6(b) terminates at $x/L = 0.16$.

Figures 5 and 6 confirm the presence of a U-shaped flow loop, downward in the outer annulus and upward in the core. Of particular note is the fact that the downflowing fluid very nearly penetrates to the surface of the liquid, whereupon it turns and sweeps across the surface as it moves radially inward. As can be seen in the figures, the evaporating vapor (represented by the streamlines which originate at the base of the tube) is swept radially inward by the circulating flow. Upon approaching the tube axis, the radial flow wells up from the liquid surface and streams upward in a tight sheath which envelops the axis.

The flow pattern revealed by the streamline maps contrasts sharply with that of the diffusion-induced flow in the Stefan problem. There, the flow is primarily axial across the entire section of the tube (wall effects are omitted because the Stefan model is one-dimensional).

Mass fraction profiles

Profiles of the vapor mass fraction W_1 are presented in Figs. 7 and 8. These figures are the counterparts of the velocity profile figures, Figs. 3 and 4. Figure 7 is for $L/R = 2$, while Fig. 8 is for $L/R = 10$. For both figures, W_{10}

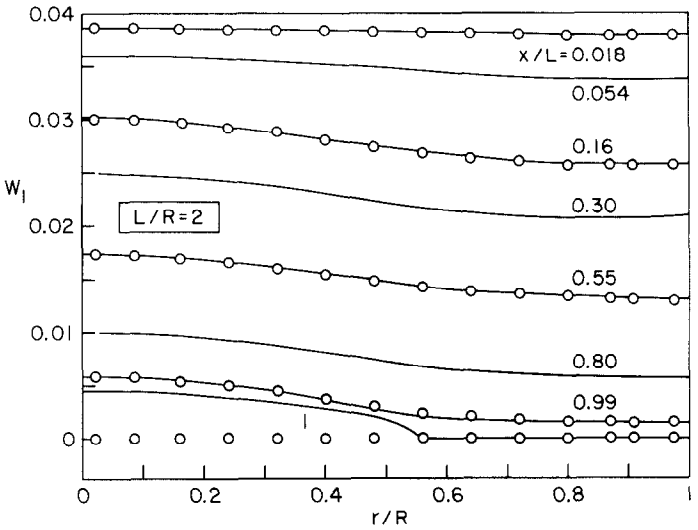

FIG. 7. Profiles of the vapor mass fraction for a tube with aspect ratio $L/R = 2$. $W_{1_0} = 0.04$, $W_{1_\infty} = 0$ and $Gr = 10^4$.

$= 0.04$, $W_{1_\infty} = 0$, and $Gr = 10^4$. In each figure, profiles are plotted at a succession of axial stations. The solid lines correspond to the inflow/outflow mass fraction closure condition, while discrete circles are used to represent the results for the uniform mass fraction closure condition.

The motivation for presenting the mass fraction results for the two closure conditions is to display the extent to which they merge. In this regard, attention may first be drawn to the W_1 profiles at the tube opening ($x/L = 1$). The profile for the uniform mass fraction closure (the circles) is horizontal and equal to $W_1 = 0$ all across the opening, and the profile for the inflow/outflow closure also passes through $W_1 = 0$ in the inflow annulus. In the core, the latter profile attains somewhat elevated values of W_1, reflecting the state of the exiting flow. However, the deviations between the two profiles virtually disappear at $x/L = 0.99$, which is immediately adjacent to the opening. At the other axial stations at which comparisons are made, the two profiles are nearly congruent.

The very rapid adjustment experienced by the W_1 profiles for the uniform mass fraction closure in order to match those for the inflow/outflow closure suggests that the latter may be more in tune with the physics of the problem. Since the buoyancy forces which drive the natural convection are intimately related to the mass fraction distribution, the results of Figs. 7 and 8 explain why the two closure conditions yielded virtually the same evaporation rates.

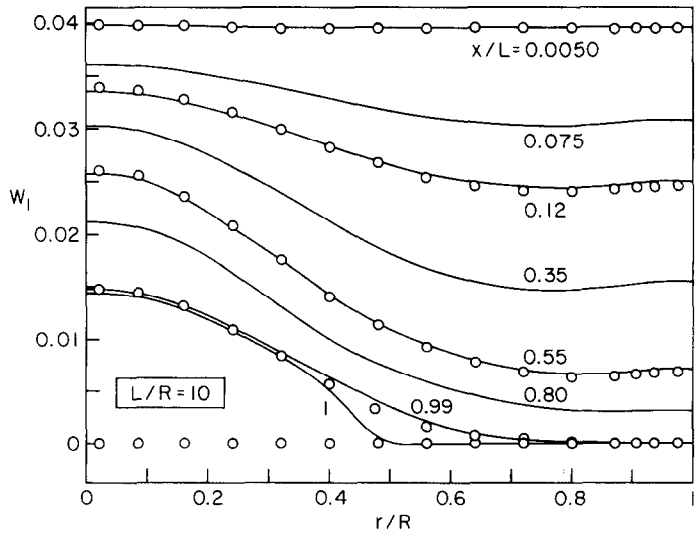

FIG. 8. Profiles of the vapor mass fraction for a tube with aspect ratio $L/R = 10$. $W_{1_0} = 0.04$, $W_{1_\infty} = 0$ and $Gr = 10^4$.

Further inspection of Figs. 7 and 8 shows that at any axial station, the vapor mass fraction decreases from the tube axis to the wall. This trend is in accord with the flow patterns illustrated in Figs. 5 and 6. The extent of the radial variations is accentuated for longer tubes, as can be verified by comparing Figs. 7 and 8.

CONCLUDING REMARKS

An analysis has been performed of evaporation in the presence of natural convection. The evaporating liquid partially fills a vertical tube whose upper end is open to a fluid environment consisting either of a pure gas or of a binary mixture of a gas and the vapor of the evaporating liquid. The entire system is isothermal, and the natural convection is driven by density variations which are due to spatial variations of the concentrations of the species (i.e. the gas and the vapor). To establish a decrease of the density in the upward vertical direction, as required for the existence of the natural convection, the molecular weight of the evaporating vapor must be lower than that of the gas. This condition is fulfilled when water is the vapor and air is the gas, and the numerical work was performed for the water–air system.

It was found that the presence of natural convection can lead to significant increases in the rate of evaporation—up to a factor of five for the investigated parameter ranges. The enhancement of the evaporation rate due to natural convection was favored by a relatively high concentration of vapor at the liquid surface, a dry ambient, and a relatively large tube radius. For such conditions, it is inappropriate to predict the evaporation rate from the Stefan diffusion model, which neglects natural convection.

The natural convection sets up a U-shaped flow loop. The downflow leg of the loop is formed by fluid from the ambient which is drawn into the tube through an annular region situated adjacent to the tube wall. The upstreaming fluid which occupies the core of the tube forms the other leg of the loop.

REFERENCES

1. E. R. G. Eckert and R. M. Drake, Jr, *Heat and Mass Transfer*. McGraw-Hill, New York (1959).
2. R. B. Bird, W. E. Stewart and E. N. Lightfoot, *Transport Phenomena*. Wiley, New York (1960).
3. L. C. Burmeister, *Convective Heat Transfer*. Wiley, New York (1983).
4. T. K. Sherwood, R. L. Pigford and C. R. Wilke, *Mass Transfer*. McGraw-Hill, New York (1975).
5. C. Y. Lee and C. R. Wilke, Measurement of vapor diffusion coefficient, *Ind. Engng Chem.* **46,** 2381–2387 (1954).
6. J. M. Pommersheim and B. A. Ranck, Measurement of gaseous diffusion coefficients using the Stefan cell, *Ind. Engng Chem. Fundam.* **12,** 246–250 (1973).
7. B. L. Markham and F. Rosenberger, Velocity and concentration in a Stefan diffusion tube, *Chem. Engng Commun.* **5,** 287–298 (1980).
8. S. Whitaker, Velocity profile in the Stefan diffusion tube, *Ind. Engng Chem. Fundam.* **6,** 476 (1967).
9. S. V. Patankar, *Numerical Heat Transfer and Fluid Flow*. Hemisphere, Washington, D.C. (1980).
10. C. Prakash and S. V. Patankar, Combined free and forced convection in vertical tubes with radial internal fins, *J. Heat Transfer* **103,** 566–572 (1981).

ANALYSE DE L'EVAPORATION EN PRESENCE DE CONVECTION NATURELLE INDUITE PAR LA COMPOSITION MASSIQUE

Résumé—On étudie analytiquement et numériquement l'évaporation à partir d'un tube ouvert à la partie supérieure et partiellement rempli avec un liquide. L'espace au dessus de la surface libre est occupé par un mélange binaire d'une vapeur évaporée et d'un gaz. Les variations spatiales des concentrations de la vapeur et du gaz provoquent des variations de densité qui induisent des mouvements de convection naturelle. Les solutions numériques sont menées pour l'eau comme évaporant et l'air pour gaz. On trouve que la présence de convection naturelle peut conduire à des accroissements sensibles du taux d'évaporation, jusqu'à un facteur cinq dans les domaines étudiés. L'accroissement est favorisé par une concentration relativement élevée de vapeur à la surface du liquide, une ambiance séche, et un diamètre relativement grand du tube. La configuration de l'écoulement consiste en une boucle en forme de U, avec le fluide poussé vers le bas dans le tube depuis l'ambiance, à travers une région annulaire adjacente à la paroi du tube. L'écoulement ascendant dans le coeur du tube forme l'autre branche de la boucle.

VERDAMPFUNGSUNTERSUCHUNG BEIM AUFTRETEN VON ZUSAMMENSETZUNGSBEDINGTER NATÜRLICHER KONVEKTION

Zusammenfassung—Die Verdampfung in einem oben offenen senkrechten Rohr, welches zum Teil mit einer Flüssigkeit gefüllt ist, wurde analytisch und numerisch untersucht. Im Raum oberhalb der Flüssigkeitsoberfläche befindet sich ein binäres Gemisch aus verdampfter Flüssigkeit und einem Gas. Räumliche Konzentrationsänderung des Dampfes und des Gases verursachen Dichteunterschiede, welche natürliche Konvektions bewegungen hervorrufen. Die numerischen Lösungen wurden mit Wasser als zu verdampfendes Medium und Luft als Gas durchgeführt. Es wurde herausgefunden, daß bei Anwesenheit von natürlicher Konvektion die Verdampfungsrate signifikant—bis zu einem Faktor 5 bei den untersuchten Parametern—zunimmt. Die Verbesserung wird durch eine relativ große Dampfkonzentration an der Flüssigkeitsoberfläche, durch eine trockene Umgebung und einen relativ großen Rohrdurchmesser begünstigt. Das Strömungsbild ist U-förmig, wobei Fluid aus der Umgebung in einem Ringraum an der Rohrwand nach unten gezogen wird. Die Aufwärtsströmung in der Rohrmitte bildet den anderen Schenkel der U-förmigen Strömung.

АНАЛИЗ ИСПАРЕНИЯ В ПРИСУТСТВИИ КОНЦЕНТРАЦИОННОЙ КОНВЕКЦИИ

Аннотация—Аналитически и численно исследовано испарение с открытого верхнего торца вертикальной трубы, частично занятой жидкостью. Пространство над поверхностью жидкости заполнено бинарной смесью, состоящей из испаряющегося пара и газа. Пространственные изменения концентрации пара и газа приводят к изменениям плотности, вызывающим конвективное движение. Численные решения проведены для водяного пара и воздуха. Найдено, что естественная конвекция может привести к существенному увеличению скорости испарения—в пять раз для исследованных условий. Такое увеличение обусловлено относительно высокой концентрацией пара на поверхности жидкости, сухой окружающей средой и относительно большим диаметром трубы. Структура течения представляет собой U-образный контур, в котором смесь из окружающей среды опускается по трубе через кольцевую область, прилегающую к стенке трубы. Подъемное течение в центральной части трубы образует другую ветвь контура.